

B 7 Dynamics of Glass Forming Polymers – Computer Simulation and Neutron Scattering

D. Richter

Institut für Festkörperforschung

Forschungszentrum Jülich GmbH

Contents

1	Introduction	2
2	Neutron scattering principles.....	2
3	Simulations procedures	4
4	Neutron scattering techniques	5
5	Relaxation processes in polymers	6
5.1	The structural or α -relaxation	8
5.1.1	Neutron scattering experiments [5,6].....	10
5.1.2	Molecular dynamics simulations [7].....	12
5.1.3	Interpretation within a simple model [5,6]	17
5.2	Local dynamics [11]	19
6	Summary and conclusions.....	23

1 Introduction

Neutron scattering and computational techniques are highly complementary for one simple reason. From a model of atomic positions possibly as a function of time it is straight forward to calculate the expected neutron scattering spectrum and to compare it to experimental results on an absolute scale. There are no unknown or difficult to calculate coupling functions, neutron scattering therefore provides the best method for testing and benchmarking computational methods like e.g. Monte Carlo and molecular dynamic simulations.

In this lecture we will first address some principles of neutron scattering, will then briefly describe molecular dynamic simulations done by commercial software and then address results on primary and secondary relaxations of glass forming polyisoprene and polybutadiene. Using measurements of the quasielastic neutron spectra as a function of momentum transfer, we will benchmark computer simulation and then gain deeper insights into the underlying dynamics in exploiting the detailed information provided by the space time dependent trajectories available in computer simulation. In the case of the secondary relaxation we will use concepts developed to model scattering spectra now in real space, in order to extract more detailed insight from simulated correlation functions.

2 Neutron scattering principles

The velocity of neutrons has the same order of magnitude as the atomic velocities in condensed matter. Therefore even slow relaxational motions are detectable by a velocity change of the neutron. The spatial character of the motion then is inferred from the angular distribution of the scattered neutrons.

In general scattering of thermal neutrons yields information on the sample by a measurement and analysis of the double differential cross section .

$$\frac{d\sigma(\theta)}{d\Omega dE} = \frac{k_f}{k_i} \frac{1}{N} \sum_{i,j} \langle b_i b_j \rangle S_{i,j}(\underline{Q}, \omega) \quad (1)$$

I.e. the intensity of scattered neutrons with energy E_f into a given direction θ . The energy transfer, i.e. the difference of kinetic energy before and after scattering $\Delta E = E_f - E_i$ relates to $\omega E = \frac{\Delta E}{\hbar}$.

The momentum transfer $\hbar \underline{Q}$ respectively the scattering wave vector is given by $\underline{Q} = \underline{k}_i - \underline{k}_f$ where \underline{k}_i and \underline{k}_f are the wave vectors of the incoming and outgoing (scattered) neutrons. They relate to the neutron wave lengths $|\underline{k}_{i,f}| = \frac{2\pi}{\lambda_{i,f}}$ the neutron momentum are $\underline{p}_{i,f} = m_n \underline{v}_{i,f} = \hbar \underline{k}_{i,f}$.

Therefore

$$\omega = \frac{\Delta E}{\hbar} = \frac{(p_f^2 - p_i^2)}{(2\hbar m_n)} \quad (2)$$

the energy ΔE and ω can be determined by measurements of the neutron velocities v_i and v_f . Note that for all problems we will discuss in this lecture $k_i \cong k_f$ and therefore

$$Q = \frac{4\pi}{\lambda_i} \sin\left(\frac{\theta}{2}\right) = 2|k_i| \sin\left(\frac{\theta}{2}\right) \quad (3)$$

can be assumed. Finally, b_i denotes the scattering length of atom nucleus i and $\langle \dots \rangle$ is the assemble average.

The unique features of neutrons that render them into a powerful tool for the investigations of polymers are

- the isotope and spin dependence of b_i ,
- typical wavelength of cold and thermal neutrons, that match molecular and atomic distances and
- even slow motions of molecules cause neutron velocity changes that are large enough to be detectable.

In particular neutron spin echo spectroscopy is able to resolve changes Δv of the order of $10^{-5} v_i$.

In order to proceed further we introduce the intermediate scattering function as the Fourier transform of $S(Q, \omega)$:

$$S(\underline{Q}, t) = \int_{-\infty}^{\infty} S(\underline{Q}, \omega) e^{i\omega t} d\omega \quad (4)$$

The intermediate scattering function directly depends on the (time dependent atomic positions).

$$S_{ij}(\underline{Q}, t) = \left\langle \sum_{n,m} e^{i\underline{Q} \cdot [\underline{r}_n^i(t) - \underline{r}_m^j]} \right\rangle \quad (5)$$

Note that Eq.[5] relates the experimental accessible scattering function directly to the time dependent atomic coordinates which are accessible to computer simulation, establishing thereby the quoted important relationship between simulation and neutron scattering.

Considering the ensemble average of Eq.[1] we have to consider that chemically equivalent atoms may have a number of different scattering lengths that are randomly distributed over the ensemble of all atoms of the same kind in the sample. Most important in the present context is the variation due to the spin dependent component of the proton scattering length, where is the average value $\langle b_i \rangle$ leads to the coherent scattering, the fluctuating part $b_i - \langle b_i \rangle$ leads to incoherent scattering i.e. scattering, which is not giving rise to constructive

interference and therefore yields as an additional contribution, the atom-atom self correlation function.

$$S_i^{self}(\underline{Q}, t) = \left\langle e^{i\underline{Q}(\underline{r}_i(t) - \underline{r}_i(0))} \right\rangle \quad (6)$$

Note, that in Eq.[6] the coordinate of the same atom appears at different times. Therefore S_i^{self} informs about the motion of a given atom. Applying the Gaussian approximation i.e. assuming that the atomic displacement distribution functions are Gaussian, Eq.[6] transforms into

$$S^{self}(Q, t) = \exp\left(-\frac{Q^2}{6} \langle r_i^2(t) \rangle\right) \quad (7)$$

where $\langle r_i^2(t) \rangle$ is the mean square displacement of atom “i”. This quantity again is directly accessible to simulations and facilitates a direct comparison between neutron scattering and simulation results. In this lecture we will only discuss isotropic samples. Therefore in the following we only need to consider the magnitude of Q but not its direction.

We further remark that (i) the scattering length of hydrogen and deuterium are very different, facilitating a specific labelling of certain molecules or molecular components and (ii) that the magnitude of the incoherent scattering from hydrogen is significantly larger than that of deuterium or carbon and therefore outside the range of small angle scattering, the incoherent scattering from hydrogen dominates the spectra and providing a means to selectively emphasizing certain molecules or part of molecules by specific hydrogenation or deuteration.

3 Simulations procedures

All simulations which are discussed in this lecture were carried out by using the INSIGHT (INSIGHT II.4.0.0P version) and the Discover-3 module from Molecular Simulations inc. with the Polymer Consortium Force Field [1]. The functional form of this force field include terms that can be divided into two categories. Valence terms including diagonal and off-diagonal cross coupling terms and non-bonded interaction terms.

- The valence terms represent internal coordinates of the bond, angle, torsion angle and out of plane angle and the cross coupling terms include combinations of two or three internal coordinates. These cross coupling terms are important for predicting vibrational frequencies and structural variations associated with conformational changes. The analytical expression employs quartic polynomials for bond stretching and angle bending and a three term Fourier expansion for torsions.
- The non-bonded interaction terms include a columbic function for the electrostatic interaction and a Lennard-Jones 9-6 potential function rather than the more constant customary Lennard-Jones 12-6 potential for the van der Waals term.

The model systems were build by means of the well known amorphous cell protocol [2]. The amorphous cells were constructed with a given density and periodic boundary conditions are

assumed in order to model a bulk system. In the next step the energy of the so obtained structure was minimized and then subsequent dynamic runs assure a further equilibration of the structure. Typical MD runs extended between 1ns and 100ns with collecting data every one hundreds of a picosecond. The results of the MD runs were validated in comparing with actual neutron scattering results as we will discuss later.

4 Neutron scattering techniques

It is a task of inelastic neutron scattering to measure simultaneously the energy transfer $\hbar\omega$ and the momentum transfer $\hbar Q$ of the scattered neutrons. In the following we will briefly discuss two different techniques which are important for this lecture, namely backscattering and neutron spin echo .

Neutron backscattering exploits the fact, that at a scattering angle of $2\theta = 180^\circ$ the selected wavelength in reflection from a crystal depends only to second order on the divergence of the incoming beam. Choosing backreflection from a perfect crystal in combination with relaxed collimation of the neutron beam, leads to an acceptable intensity and energy resolutions in the order of 10^{-4} . Figure 1 displays the general layout of the backscattering spectrometer (BSS) at the FRJ-2 reactor in Jülich. The neutrons are monochromatized by a perfect silicon crystal, mounted on a Doppler driver which similar as in Mößbauer experiments varies the incident energy of the neutrons by a Doppler shifting. These monochromatized neutrons are deflected by a graphite crystal and directed towards the sample. The analyzer crystals are mounted on spherically hollowed plates with a radius of curvature such that they focus the reflected neutrons into detectors which are set up behind the sample. In this way, a large solid angle is covered on the analyzers side. The typical resolution achieved with this instrument is in the order of $1\mu\text{eV}$.

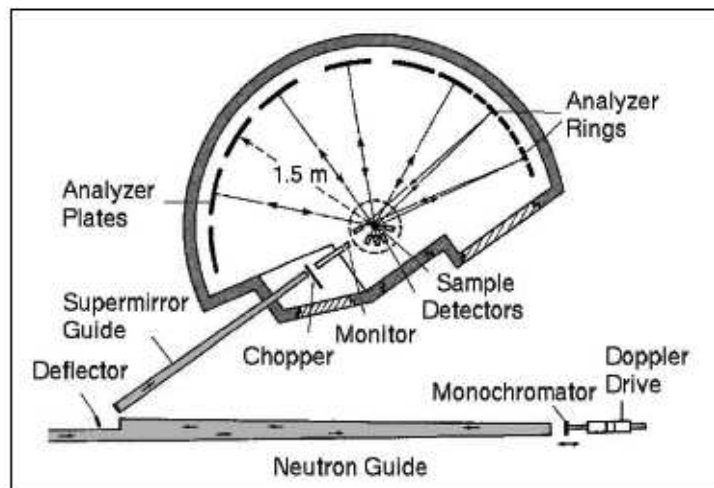


Fig. 1: Schematic sketch of the Jülich backscattering instrument BSS.

While in backscattering the energy transfer at the sample is determined by first measuring the energy of the incident neutron and thereafter that of the scattered neutron taking the difference, the unique feature of neutron spin echo (NSE) is its ability to determine energy

changes of neutrons during scattering in a direct way [3]. NSE measures the neutron velocities of the incoming and scattered neutrons utilizing the Larmor precession of the neutron spin in an external magnetic field. Since the neutron spin vector acts like the hand of an internal clock attached to each neutron which stores the result of the velocity measurements on the neutron itself, this measurement is performed for each neutron individually. Therefore, the incoming and outgoing velocities of one and the same neutron can be compared directly and a velocity difference measurement becomes possible. In this way, the energy resolution and the monochromatization of the primary beam are decoupled and an energy resolution in the order of 10^{-5} can be achieved with an incident neutron spectrum of 20% bandwidth. Figure 2 displays a photo of the Jülich NSE instrument, the salient features are the two large magnetic coils providing the Larmor precession fields before and after the sample.

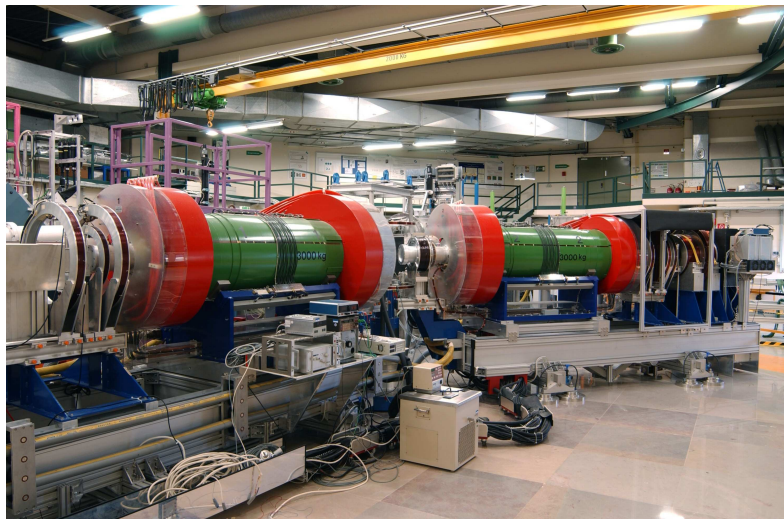


Fig. 2: Display of the Jülich Neutron Spin Echo instruments featuring the main Larmor precession coils and the sample position in between them. On the far right side the analyzer system and the detector are visible.

We note that NSE is a Fourier technique and provides directly the intermediate scattering function $S(Q,t)$ where the Fourier time t is proportional to the applied magnetic field and the third power of the wave length.

5 Relaxation processes in polymers

The classical relaxation processes in polymer, the α - and β -relaxations have been studied since more than 50 years by spectroscopic techniques like dielectric spectroscopy, mechanical spectroscopy and NMR. Figure 3 displays a typical outcome of such experiments for the case of polybutadiene (PB) ($-\text{CH}_2-\text{CH}=\text{CH}-\text{CH}_2-$)_n.

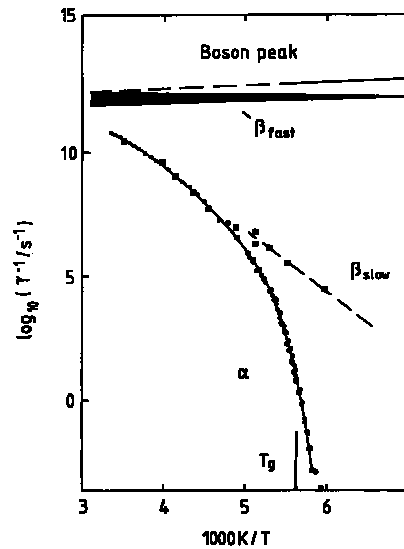


Fig. 3: Relaxation map for polybutadiene. Solid line: α -relaxation, dashed line: secondary β -process. At higher frequency the so called fast dynamics is indicated comprising the Boson peak as well as the fast relaxation.

The dominant relaxation process, the α -relaxation, is related to the macroscopic flow and freezes at a finite temperature, the glass transition temperature T_g . Aside from this process a secondary relaxation $\beta_{slow} \equiv \beta$ departs from the α branch at a temperature of about 20% above T_g . This relaxation displays an Arrhenius behaviour and passes unchanged through the glass transition. As already mentioned, the α -relaxation is at the basis of the viscous flow of polymers. Its relaxation function may be phenomenologically described by a stretched exponential function.

$$\phi_{\alpha}(t) = \exp \left\{ - \left(\frac{t}{\tau_{KWW}} \right)^{\beta} \right\} \quad (8)$$

τ_{KWW} is the Kohlrausch-Williams-Watts relaxation time and $\beta < 1$ the stretching exponent. To a good approximation, τ_{KWW} follows a Vogel-Fulcher temperature dependence

$$\tau_{KWW}(T) = \exp \left\{ \frac{B}{T - T_0} \right\} \quad (9)$$

The temperature offset in the denominator of the exponent leads to a divergence to τ_{KWW} at T_0 , a temperature below T_g which, however, never is reached in equilibrium. The dielectric β -relaxation is considered to be a result of partial reorientations of molecular building blocks in the substance. It is interpreted as a local activated process, where the dipole or the bond vector hops between positions separated by an activation energy E . Its relaxation time follows an Arrhenius behaviour

$$\tau_{\beta}(T) = \tau_0^{\beta} \exp\left[\frac{E}{k_B T}\right] \quad (10)$$

Due to the disorder in the material, the activation energies E are distributed around an average value E_0 . For the distribution function in general a Gaussian is assumed.

$$g(E) \approx \exp\left(-\frac{(E - E_0)^2}{\sigma^2}\right) \quad (11)$$

Empirically it is found that the width $\sigma(T)$ decreases with increasing temperature.

Though such processes have been investigated well by spectroscopic techniques their molecular origin is still unclear. Here we discuss a combined quasielastic neutron scattering and MD simulation approach. With their ability to provide space time resolution on the proper scales these investigations contribute to a further understanding of the molecular mechanisms behind these relaxations.

5.1 The structural or α -relaxation

As discussed above spectroscopic techniques reveal the relaxation time and the shape of the relaxation function at each temperature, while with the exception of some information on rotational processes no spatial resolutions is provided. On the other hand via the dependence on the momentum transfer, quasielastic neutron scattering (QENS) informs on the spatial evolution of relaxation processes. As an example Figure 4 presents the characteristic relaxation times for a polyisobutylene melt at different temperatures as the function of momentum transfer Q .

While in e.g. dielectric spectroscopy at each temperature one characteristic time would be revealed, QENS results in an ensemble of $\tau_{KWW}(Q)$. These relaxation times exhibit a strong dispersion which over a large range may be described by a power law $\tau_{KWW} \approx Q^{-3.6}$ [4]. Such a dispersion is a signature for a diffusive process which would be expected from the α -relaxation being at the basis of the macroscopic flow properties. The relationship between the shape of the relaxation function and its Q -dependence now allows to address the issue of heterogeneity in the dynamics of undercooled liquids and connected with it, the deviations from Gaussianity of the dynamic correlation functions.

There exists a long standing debate whether the stretched exponential shape of the α -relaxation function is a result of a superposition of heterogeneous relaxation processes in a material or whether it results from an intrinsic property of the dynamical process.

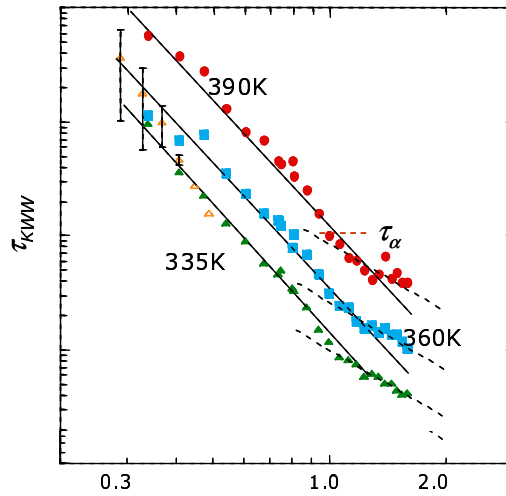


Fig. 4: Kohlrausch-Williams-Watts (KWW) relaxation times. τ_{KWW} observed for polyisobutylene at three different temperatures. The solid lines demonstrate the power law behaviour of the characteristic time. $\tau_{KWW} \approx Q^{-2/\beta}$ where β is the stretching exponent

Since a monotonous function can always be written as a Laplace transform of a non-negative function, the KWW function can easily be interpreted as arising from a superposition of different simple exponential relaxations weighted by a broad distribution of relaxation times $g(\ln \tau)$.

$$\phi(t) = \exp\left(-\left(\frac{t}{\tau_{KWW}}\right)^\beta\right) = \int_{-\infty}^{+\infty} g(\ln \tau) \exp\left(-\frac{t}{\tau}\right) d\ln \tau \quad (12)$$

This picture is usually known as the heterogeneous scenario.

The other extreme picture, the homogenous scenario considers that the atoms in the systems relax identically but by an intrinsically non-exponential process. In this scenario, the mean square displacement (MSD) is supposed to be sublinear in time $\langle r^2(t) \rangle \approx t^\beta$. Using the Gaussian assumption we may now compare Eq.[7] and Eq.[8]

$$-\frac{Q^2}{6} \langle r^2(t) \rangle = -\left(\frac{t}{\tau_{KWW}}\right)^\beta \quad (13)$$

resulting in a dispersion prediction for the Kohlrausch-Williams-Watts time .

$$\tau_{KWW} \sim Q^{-2/\beta} \quad (14)$$

Thus in the homogenous scenario there exists a prediction connecting the shape of the relaxation function characterized by the stretching exponent β and the dispersion of the characteristic time $\tau_{KWW}(Q)$. Thus, an investigation of the Q dependent spectra resulting from the α -process in a polymer melt allows to scrutinize the issue of heterogeneous vs. homogenous behaviour.

Starting from a Gaussian correlation function, the leading deviations are measured by the so called non-Gaussianity parameter

$$\alpha_2(t) = \frac{3}{5} \frac{\langle r^4(t) \rangle}{\langle r^2(t) \rangle^2} - 1 \quad (15)$$

where $\langle r^{2n} \rangle$ are moments of the selfcorrelation function $G_s(r, t)$.

5.1.1 Neutron scattering experiments [5,6]

Figure 5 presents neutron spin echo data from a monodisperse polyisoprene sample (PI d3) with deuterated methyl groups: $-(\text{CH}_2-\text{CH}=\text{C}(\text{CD}_3)-\text{CH}_2)_n-$. For such a sample the scattering is dominated by the high incoherent cross section of the hydrogens and therefore reveals the selfcorrelation function. Due to the deuteration of the methyl groups effects from the methyl group motions are avoided. The solid lines display fits with the stretched exponential functions (Eq.[8]). The spectra qualitatively display the strong dispersion of the Q dependent relaxation: while at low Q the relaxation function only decays by about 25% at higher Q values a full relaxation is observed. The lower part of Figure 5 presents a spectrum obtained with a backscattering instrument; for illustration also the experimental resolution function is indicated. All data taken at different momentum transfers and temperatures were evaluated in terms of stretched exponential functions revealing both the characteristic times as well as the respective stretching parameters.

Figure 6 displays the obtained relaxation times in the investigated Q - T regime. We note that for PI the stretching parameter changes from about $\beta = 0.4$ at $T = 280\text{K}$ to $\beta = 0.57$ at $T = 340\text{K}$. The solid lines in the upper part of Figure 6 display the predictions within the homogenous scenario (Eq.[14]). $\tau \approx Q^{-2/\beta}$. As may be seen, where experimentally accessible, the corresponding relaxation times in the low Q regime follow well this prediction. On the other hand above $Q \approx 1\text{\AA}^{-1}$ the times deviate from this behaviour and follow a weaker Q dependence. In the lower part of Figure 6 all data are condensed to a single master curve. This is done first of all by exponentiation of $\tau_{KWW}(Q)$ to the power of β . According to the Gaussian prediction $\tau_{KWW}^\beta \approx Q^{-2}$ (Eq.[14]). In this way the effect of the changing β is eliminated. Secondly, the temperature dependence is removed in applying shift factors a_T obtained from dielectric spectroscopy relative to a reference temperature T_R ($T_R = 300\text{K}$ in Figure 6).

Within experimental uncertainties all data collapse very nicely to a single master curve. A Q^{-2} dependence of τ_{KWW}^β is obtained at low Q crossing over to a weaker power law at Q around 1.3\AA^{-1} . While at low Q the dynamics of polyisoprene follows well the Gaussian prediction indicating homogenous relaxation for $Q > 1.3\text{\AA}^{-1}$ a cross over to a weaker Q dependence occurs indicating a non-Gaussian character of the α -relaxation. Indications for such a crossover are also evident in Figure 4 for data on polyisobutylene.

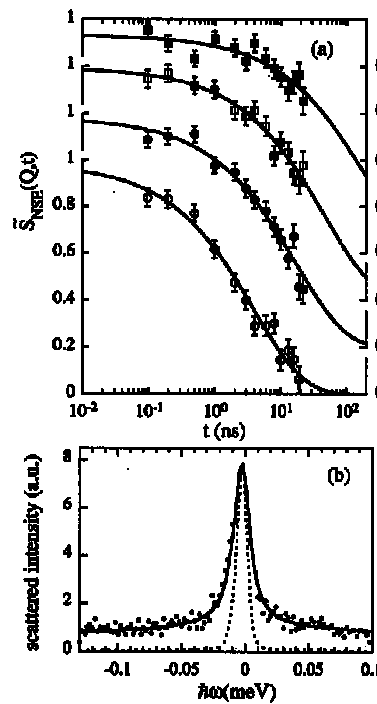


Fig. 5: Spectra obtained for PId3 (a) by the Jülich NSE at 340K and $Q = 0.10, 0.15, 0.20$, and 0.30\AA^{-1} (top to bottom), and (b) by IN13 at the ILL at 2.9\AA^{-1} and 300K. Solid lines correspond to KWW descriptions with $\beta = 0.57$ (a) and $\beta = 0.50$ (b). The dotted line shows the IN13 instrumental resolution function obtained at 1.5 K

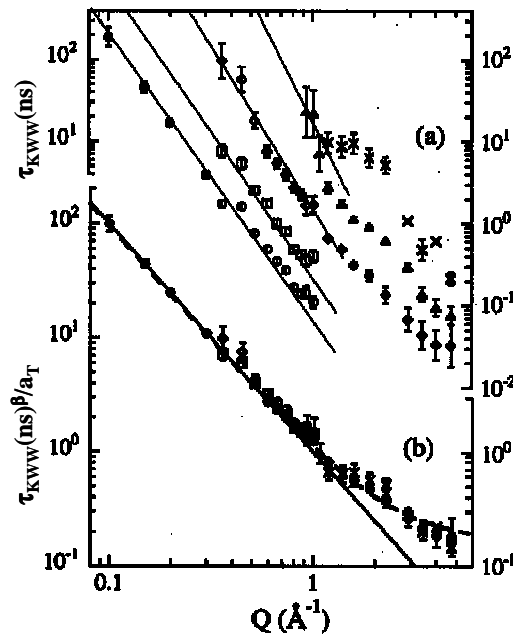


Fig. 6: (a) Q dependence of τ_w obtained for PId3 by IN13 (X: 260K; ▲: 280K; ◆: 300K), IN11c (△: 280K; ◇: 300K; □: 320K; ○: 340 K) and Jülich NSE spectrometer (●: 340K). (b) Master curve built with the data in (a) (see the text). The straight solid lines display the Q dependence expected from the Gaussian approximation. The dashed line shows the

description of the master in terms of the anomalous jump diffusion model (Eq.[22]) with $\ell_0 = 0.42\text{\AA}$.

5.1.2 Molecular dynamics simulations [7]

In order to achieve a deeper understanding of these experimental results, atomistic MD simulations are necessary. They were performed as described in section 3 for a polyisoprene chain of $N = 100$ monomers at a temperature $T = 363\text{K}$. First of all such simulations provide structural information in terms of the so called radial distribution function or its counter part, the static structure factor $S(Q)$. In the case of amorphous polymers $S(Q)$ can be measured by neutron diffraction using a fully deuterated sample, where all hydrogens are replaced by deuteriums. The cross section then follows from Eq.[5] taking the position vectors at equal times. Further information is achieved from experiments, where a part of the deuterons are replaced by hydrogens. In this way different groups of atoms are emphasized and so called partial structure factors are accessible. Figure 7 displays a comparison of simulated structure factors for 4 differently labelled PI materials with the corresponding experimental results. hPI denotes a fully protonated material, dPI the fully deuterated one, d5PI a polyisoprene with the protonated methyl group and the deuterated main chain and finally d3PI a material with a deuterated methyl group and a protonated main chain.

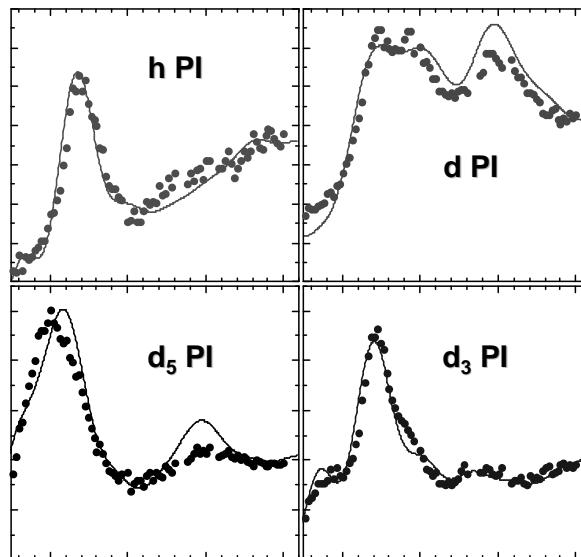


Fig. 7: Static structure factors for polyisoprene with different hd labelling. hPI: fully protonated material, dPI: fully deuterated material, d5PI: main chain deuterated polymer, d3PI: methyl group deuterated polyisoprene. The solid lines are the result of the MD simulation [8].

In all cases we observe good agreement between the simulated structure factors and the experimental counter parts indicating the basic correctness of the structure represented by the amorphous cell.

In addition to structural features we can also investigate whether the force field used in the simulations reproduces the main vibrational properties of polyisoprene at low temperatures. The vibrational density of states (VDOS), $Z(E)$ may be obtained on the one hand from

inelastic neutron scattering experiments [9]. Both for the methyl group hydrogens as well as for those from the main chain. From the MD simulations the vibrational density of states can be calculated in general as the spectral density of the velocity auto correlation function.

$$Z(E) \propto \int_{-\infty}^{+\infty} e^{-iEt} \langle \vec{v}(0) \vec{v}(t) dt \rangle \quad (16)$$

Figure 8 compares the experimental results with the MD calculation. As can be seen, there is a good agreement between the simulation and the experimental data sets, at least in the energy range $E \leq 40 \text{ meV}$, where experimental data are available. Beyond the neutron results the simulated $Z(E)$ also shows maxima at higher energies. Though quantum effects certainly affect the high energy range of $Z(E)$ the obtained maxima correspond rather well with different infrared bands reported for PI. Thus, in addition to the amorphous structure also the vibrational properties of PI are well depicted by the simulations.

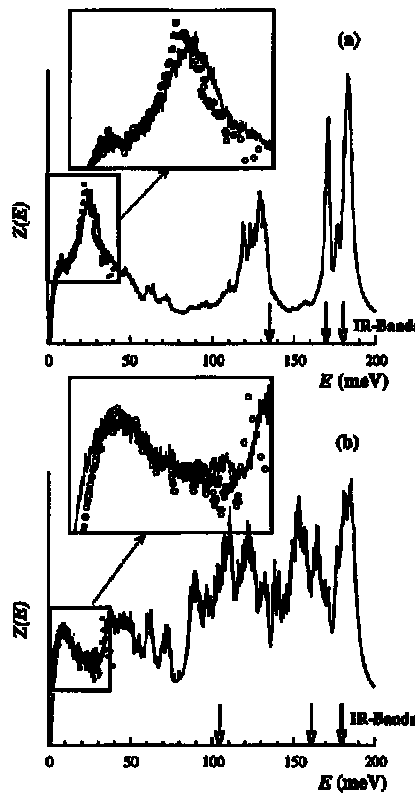


Fig. 8: Vibrational density of states of the methyl group hydrogens (a) and main chain hydrogens (b) as obtained for PI from inelastic neutron scattering measurements (\circ) and from our MD simulations (solid lines). The arrows show the energy of some infrared bands.

From the atomic trajectories in the simulations also the selfcorrelation function may be calculated directly. Assuming isotropic behaviour this function is given by

$$G_s(r, t) = \frac{1}{N} \left\langle \sum_{i=1}^N \delta[r - |\vec{r}_i(t) - \vec{r}_i(0)|] \right\rangle \quad (17)$$

where r is the radial distance from a given particle. N is the number of particles and r_i is the position vector of the i 's particle. The angular brackets denote canonical averaging. $G_s(r,t)$ is related to Eq.[6] through Fourier transformation. In the simplest case the self correlation function can be approximated by a Gaussian function.

$$G_s^{gaus}(r,t) = \left[\frac{\alpha(t)}{\pi} \right]^{3/2} \exp[-\alpha(t)r^2] \quad (18)$$

This form holds rigorously for an ideal gas, for harmonic crystal and for a system where the motion of the atom is governed by Langevin equations. First order deviations from this form are characterized by the above mentioned non-Gaussianity parameter α_2 (Eq.[15]). If $G_s(r,t)$ is strictly Gaussian, $\alpha_2(t)$ is 0 and $\langle r^2(t) \rangle = 3/(2\alpha(t))$.

Figure 9 displays the simulated Fourier transformed selfcorrelation function for different momentum transfers Q . $S^{self}(Q,t)$ exhibits a two step decay which is characteristic of glass forming supercooled liquids in general. The initial decay takes place at times below 1ps and corresponds to the so called fast dynamics in glass forming materials. It is outside the observation window of the discussed experiments and therefore we will focus here on the slower decay of S^{self} which relates to the α -relaxation. The solid lines in Figure 9 present fits with a stretched exponentials to the data. Thereby a Q dependent prefactor was considered in order to account for the initial fast decay.

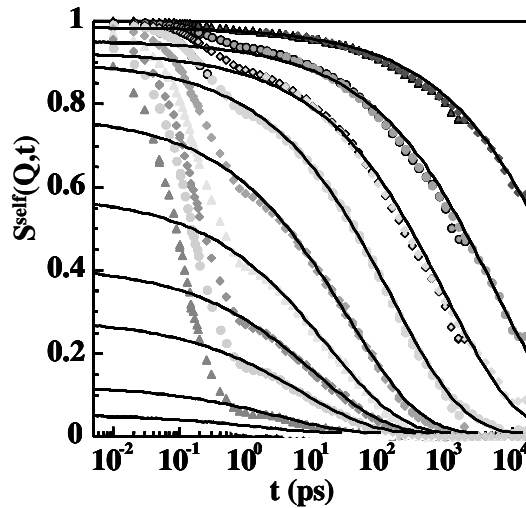


Fig. 9: Incoherent intermediate scattering function obtained by MD simulation for polyisoprene at $T = 363K$. The structure factor is given from above for $Q = 0.3, 0.5, 0.7, 1.0, 1.5, 2.0, 2.5, 3.0, 4.0$ and 5.0 \AA^{-1} for the main chain protons for polyisoprene. The solid lines are the curves corresponding to a fit of the data with a stretched exponentials for times $t \geq 5ps$.

Figure 10 displays the resulting $\tau_{KWW}(Q)$. As the experimental results which were displayed in Figure 6, also the simulated data display a clear cross over from a Gaussian regime at low Q to a non-Gaussian range at higher Q . Figure 10b compares the simulation results with the condensed experimental data of Figure 6. Thereby again we have exponentiated all data with

the stretching exponent β in order to remove the influence of the different stretching of the relaxation curves. As may be seen, both the experimental as well as the simulated characteristic times agree exceptionally well.

In order to address the question of Gaussianity more deeply, the simulation results were also used in order to calculate the non-Gaussianity parameter α_2 (Eq.[15]) which may be obtained from calculating the moments of Eq.[17]. The results are displayed in Figure 11 together with the mean square displacement of the main chain protons. $\langle r^2(t) \rangle$ displays three typical dynamic ranges:

- (i) a microscopic regime until about 1ps,
- (ii) a cross over regime until about 10ps and
- (iii) a sublinear time dependence extending until the limit of the simulations (20ns).

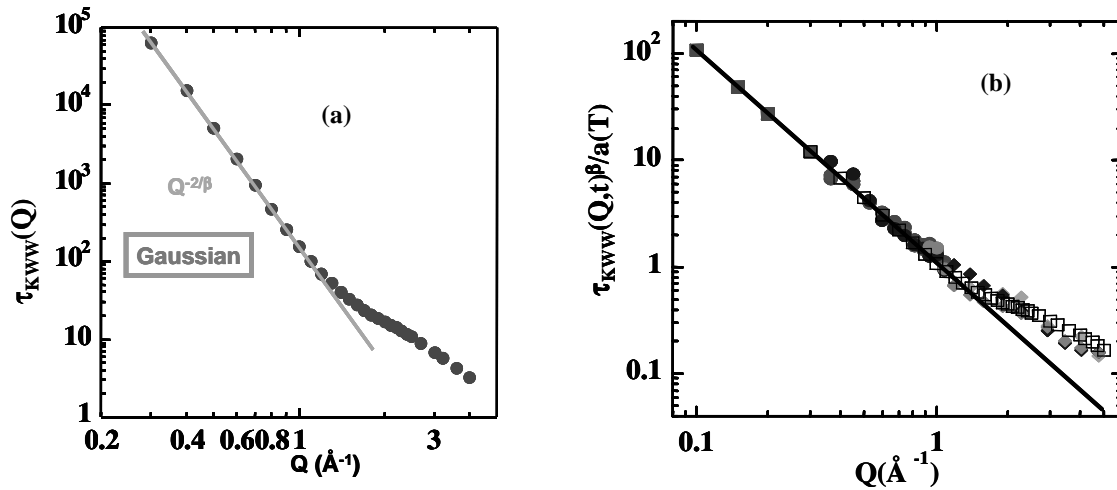


Fig. 10: (a) Dispersion of the simulated Kohlrausch-Williams-Watts time $\tau_{KWW}(Q)$ as a function of Q . The solid line displays the $Q^{-2/\beta}$ law valid for homogenous dynamics. (b) Comparison with the experimental master curve (Figure 6b). For this purpose the τ_{KWW} times were exponentiated to the power of β . The solid line indicates a Q^{-2} law. Open symbols: simulation, full symbols: experimental points

$\alpha_2(t)$ displays a double peak structure, where the short time maximum corresponds to the microscopic regime of $\langle r^2(t) \rangle$ and another is centered in the cross over regime of the MSD. While the short time peak is atom specific and appears to relate to the librational motions of the CH bonds, the second peak of $\alpha_2(t)$ shows a similar behaviour to that observed in computer simulations of Lennard-Jones systems. It shows a maximum at $t^* \sim 4$ ps centered in the cross over regime of $\langle r^2(t) \rangle$. Once the sublinear behaviour of the MSD is well established $\alpha_2(t)$ decreases to its long time limit zero.

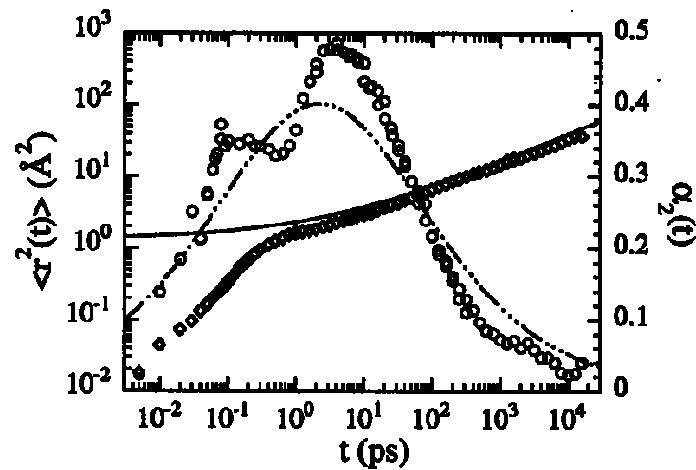


Fig. 11: Time evolution of $\langle r^2 \rangle$ (◇) and α_2 (○) obtained from the simulations at 363K for the main chain protons. The anomalous jump diffusion model with the parameters deduced from the experimental data at 320K yields the functions displayed as lines: solid for $\langle r^2 \rangle$ and dash-dotted for α_2 [5,6].

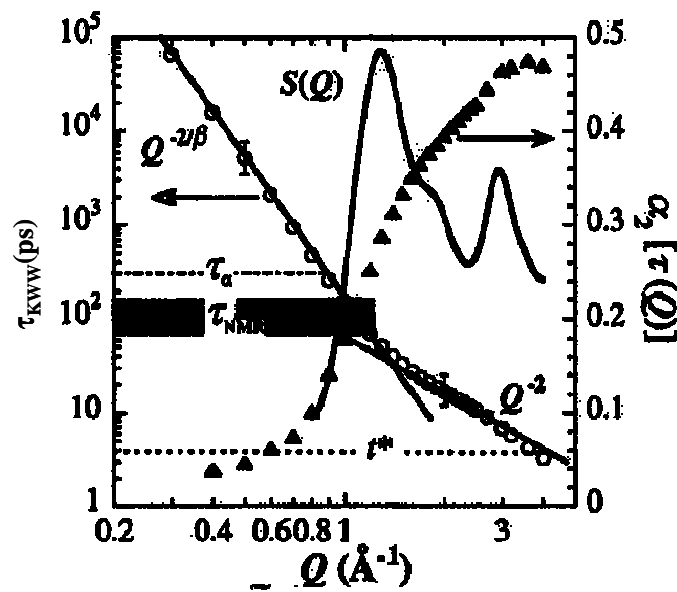


Fig. 12: Momentum transfer Q dependence of the characteristic time $\tau_{\text{KWW}}(Q)$ of the α -relaxation obtained from the slow decay of the incoherent intermediate scattering function of the main chain protons (○). The solid lines through the points show the Q dependences of $\tau_{\text{KWW}}(Q)$ indicated. The estimated error bars are shown for two Q values. The Q dependence of the value of the non-Gaussian parameter at $\tau_{\text{KWW}}(Q)$ is also included (▲) as well as the static structure factor $S(Q)$ on the linear scale in arbitrary units. The horizontal shaded area marks the range of the characteristic times τ_{NMR} . The values of τ_a and t^* are indicated by the dashed-dotted and dotted lines, respectively (see the text for the definitions of the time scales). The temperature is 363K in all cases.

How to relate the non-Gaussianity parameter with the observed Q -dependence of τ_{KWW} ? For this purpose we compare the observed dispersion $\tau_{KWW}(Q)$ with the value of α_2 at the corresponding Q -dependent correlation time. This comparison is displayed in Figure 12. At low Q where we observe $\tau \approx Q^{-2/\beta}$ the value of α_2 is very low indicating a Gaussian correlation function. Around $Q \approx 0.8 \text{ \AA}^{-1}$ α_2 is rising and reaches a value of about 0.25 in the regime where the crossover in Q occurs. The high Q non-Gaussian regime expresses itself both in strong deviations from the $Q^{-2/\beta}$ law as well as in high values of α_2 . For illustration we have also included the structural relaxation time τ_α i.e. the time at which the structure factor at its maximum relaxes, as well as the range of typical NMR relaxation times which may be computed from bond vector relaxations. Finally, we note that typical α -relaxation times observed with dielectric spectroscopy correspond to correlation times observed with neutrons at a Q value of about $Q = 1 \text{ \AA}^{-1}$. Thus, spectroscopic techniques always relate to characteristic times in a range where the non-Gaussianity parameter already is non-negligible. This may explain why e.g. NMR techniques reveal heterogeneous contributions which are absent in the low Q neutron data [10].

5.1.3 Interpretation within a simple model [5,6]

As was outlined above the characteristic times from the different spectroscopic techniques are observed in a time range where the non-Gaussianity parameter α_2 is already non-negligible and therefore those results should be more sensitive to heterogeneous dynamics. On the other hand we note that in most of the studies which invoke the concept of dynamic heterogeneity, the origin of non-vanishing values of α_2 is usually concentrated with the origin of the non-exponential behaviour of the α -relaxation, i.e. the stretching of the relaxation function.

In the following we will show that within a simple model considering finite jumps of the atoms in the α -process all observed features may be naturally explained.

In jump diffusion models finite jump length tend to cause a bending of the dispersion for the diffusive relaxation times away from the Q^{-2} which is valid for simple diffusion at low Q . The jump diffusion model assumes that an atom remains at a given site for a time τ_0 where it moves around a center of equilibrium. After τ_0 it moves rapidly to a new position located at a distance ℓ with respect to the original site. For such a process the incoherent intermediate scattering function assumes the form

$$S_{JD}^{self}(Q, t) = \exp \left[-\frac{\langle u^2 \rangle}{3} Q^2 - b(Q) \left(\frac{t}{\tau} \right)^\beta \right] \quad (\beta=1) \quad (19)$$

where $b(Q)$ depends on the particular jump geometry and $\langle u^2 \rangle$ is the vibrational MSD. Assuming randomly oriented jump direction with an exponential distribution of jump lengths

$$f_0(\ell) = \frac{\ell}{\ell_0^2} \exp \left(-\frac{\ell}{\ell_0} \right) \quad (20)$$

where ℓ_0 is the most likely jump distance.

$$b(Q) = \frac{Q^2 \ell_0^2}{(1 + Q^2 \ell_0^2)} \quad (21)$$

We note that for $Q\ell_0 \rightarrow 0$, $b(Q) \rightarrow Q^2 \ell_0^2$. In that limit $S_{jd}^{self}(Q, t)$ has a Gaussian form with an associated MSD that increases linearly with time. In glass forming systems $S^{self}(Q, t)$ exhibits the form of stretched exponential (Eq.[7,8]). An incoherent scattering function analogous to that for the simple jump diffusion (Eq.[19]) may be constructed by introducing the stretching in the time dependent part ($\beta < 1$). In this way in the limit $Q\ell_0 \rightarrow 0$ the Gaussian approximation is recuperated (see Eqs.[13,14]) but now a sublinearly increasing MSD would be obtained for small Q values as observed from experiments and simulations. By comparing Eq.[7] and [19] we obtain for τ_{KWW}

$$\tau_{KWW}(Q) = \tau_0 \left[1 + \frac{1}{Q^2 \ell_0^2} \right]^{1/\beta} \quad (22)$$

As displayed in Figure 6b, Eq.[22] provides a good description of the experimental results (dashed line). At $T_R = 300\text{K}$ we find $\tau_0 = 28\text{ps}$ and $\ell_0 = 0.42\text{\AA}$, the latter being T independent within the uncertainties. Obviously the experimentally observed Q dependence of τ_{KWW} is compatible with a scenario of sublinear diffusion for the segmental relaxation with an underlying distribution of elemental jump lengths with a most probable value of $\ell_0 \sim 0.4\text{\AA}$. From Figure 12 we have seen that deviations of $\tau_{KWW}(Q)$ from the Gaussian $Q^{-2/\beta}$ law set in if $\tau_{KWW}(Q)$ reaches a time regime where $\alpha_2(t)$ becomes significantly different from zero.

Within the jump diffusion approach α_2 may be calculated straight forwardly. Starting from Eq.[19] and inserting Eq.[21] we may expand with respect to $Q^2 \ell_0^2$. The result may be directly compared with a general expression for the expansion of $S^{self}(Q, t)$ with respect to Q .

$$S^{self}(Q, t) = \exp \left[-\frac{\langle r^2(t) \rangle}{\sigma} Q^2 + \frac{\alpha_2}{72} Q^4 \langle r^2(t) \rangle^2 + \dots \right] \quad (23)$$

revealing

$$\langle r^2(t) \rangle = 2\langle u^2 \rangle + 6\ell_0^2 \left(\frac{t}{\tau_0} \right)^\beta \quad (24)$$

and

$$\alpha_2(t) = \frac{72 \ell_0^4 \left(\frac{t}{\tau_0}\right)^\beta}{\left[2 \langle u^2 \rangle + 6 \ell_0^2 \left(\frac{t}{\tau_0}\right)^\beta\right]^2} \quad (25)$$

Using the experimental value for $\langle u^2 \rangle$, α_2 and the mean square displacement may be calculated. The results are displayed in Figure 11 as solid and dashed dotted lines. We note that for simulation times longer than microscopic times the simple models reveals very similar results as the MD simulations. This good agreement suggests that at least to a reasonable approximation the non-Gaussianity observed for the α process at short enough times finds a simple explanation in terms of a sublinear diffusion process with a distribution of finite jump length. This process is heterogeneous at short length scales and (high Q) becomes homogenous at larger scales (low Q).

5.2 Local dynamics [11]

In this chapter we will show that a real space analysis of the correlation functions obtained by MD simulations may reveal more clear and definite results than an evaluation in Fourier space. We demonstrate this approach in order to scrutinize contradictory experimental results on polybutadiene (PB) in the neighbourhood of its glass transition. PB is a simple main chain glass forming polymer with a glass transition temperature $T_g = 178\text{K}$. Aside of the α -relaxation several additional processes were identified experimentally. At 200K the following observations are reported:

- dielectric spectroscopy reveals a secondary relaxation with a characteristic time of 430ns.
- from the damping of longitudinal Brillouin modes a relaxation process at a time of 2ns was deduced.
- the dynamic structure factor $S(Q,t)$ from NSE spectroscopy indicated a secondary relaxation at 19ns.
- depolarized Raman scattering indicates a relaxation process at 0.3ns.

Simulations were performed on PB exhibiting a microstructure as in the experiment (39% cis, 58% trans, 8% vinyl; see Figure 14) using again the amorphous cell protocol. This time equilibration was performed first at $T_g + 100\text{K}$, then the temperature was gradually lowered to 200K performing density and energy equilibration runs and finally a 100ns MD simulation for further equilibration. The presented MD data stem from a 160ns run. Finally a further 300ns run confirmed the absence of aging phenomena.

The simulations were validated in comparing to the collective dynamic structure factor $S(Q,t)$ (see Eq.[5] where a sum over all atoms species has to be performed). Figure 13 displays the comparison between simulation and the corresponding NSE experiment at 200K for different Q values. As may be seen the simulations well reproduce the experimental findings.

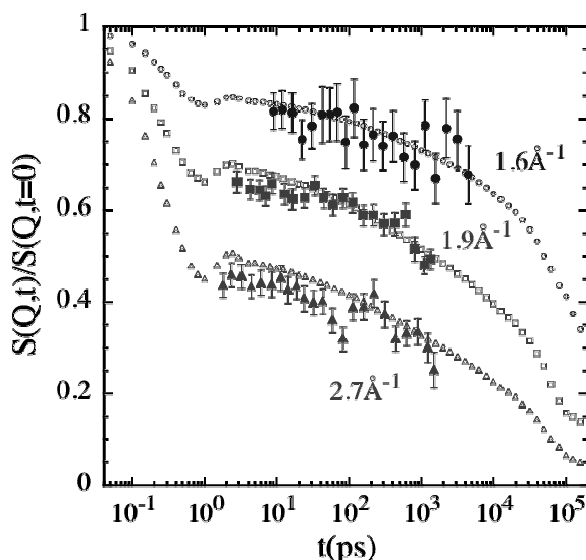


Fig. 13: Dynamic structure factor obtained for PB at 200K by NSE (full symbols) and MD simulations (empty symbols). Circles: 1.6\AA^{-1} , squares: 1.9\AA^{-1} and triangles: 2.7\AA^{-1} . The NSE amplitudes have been corrected for bandpass effects.

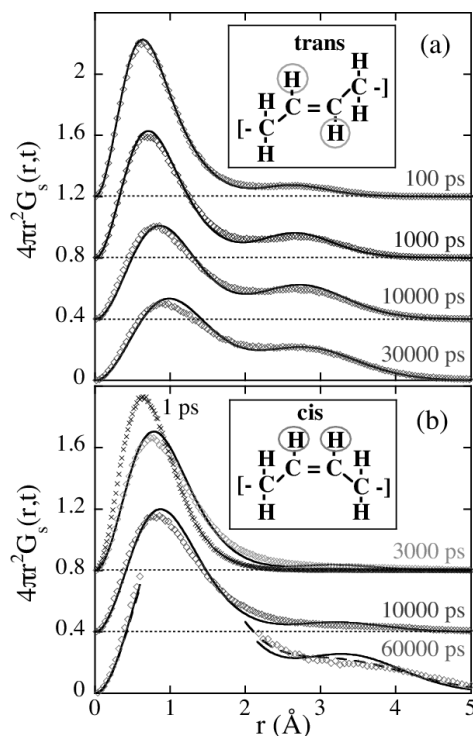


Fig. 14: Radial selfcorrelation function for the double-bond hydrogens of the trans units (a) and the cis units (b) at 200K and different times as indicated. For clarity, the origins are shifted to the levels displayed by the horizontal dotted lines. For comparison in (b) we also display the results at $t = 1\text{ps}$ (\times). The solid lines show the description obtained by the proposed model (see text). For $t = 60000\text{ps}$ in (b) we have magnified the curves such as to show the effect of a distribution of jump distances on the quality of the data description (dashed line).

Now we focus on the hydrogen selfcorrelation functions which may be measured by incoherent neutron scattering in reciprocal Q space. Here we will evaluate the MD simulations directly in real space. Figure 14 displays the radial selfcorrelation function $4\pi^2 G_s(r, t)$ at different times for the two type of hydrogen sites showing the most diverse behaviour:

- (a) at the double bond in the trans conformation ($1H_{trans}$) and
- (b) at the double bond in cis conformation ($1H_{cis}$).

Their different dynamic behaviour is striking. Aside from some diffusive broadening already at early times (100ps) the selfcorrelation function for $1H_{trans}$ (Figure 14a) develops a well resolved second maximum at $r \cong 2.7\text{\AA}$ that displays a stable growth with time. The evolution of this peak indicates a well defined hopping process which is significantly faster than the overall diffusion. In contrast the selfcorrelation function for $1H_{cis}$ (Figure 14b) is dominated by the overall diffusive broadening which as for $1H_{trans}$ leads to a slight shift of the first peak with time. In addition at later times ($t > 3000\text{ps}$) a weak shoulder at $r \cong 3\text{-}4\text{\AA}$ evolves indicating a much slower jump process.

We now consider a simple model depicting the essential features of the observed dynamics. We consider the hydrogen atoms hopping in an asymmetric double well potential. At the same time it undergoes sublinear diffusion. The hopping process is characterized by a jump distance d and a distribution of hopping times which is modelled by a stretched exponential with a characteristic time τ_{hop} and a stretching exponent β_{hop} . The sublinear or anomalous diffusion is represented by diffusion coefficient D and the stretching exponent β_{diff} . Finally, the asymmetry of the potential is depicted by the asymmetry energy ΔE . In terms of this model the selfcorrelation function may be written as

$$G_s(r, t) = \left(\eta_1^2 + \eta_2^2 + 2\eta_1\eta_2 e^{-\left(\frac{t}{\tau_{hop}}\right)^{\beta_{hop}}} \right) G_s^{diff}(r, t) + 2\eta_1\eta_2 \left(1 - e^{-\left(\frac{t}{\tau_{hop}}\right)^{\beta_{hop}}} \right) G_s^{diff}(r - d, t) \quad (26)$$

With the thermal occupation factors $\eta_1 = \left[1 + \exp\left[-\frac{\Delta E}{k_B T}\right] \right]^{-1}$; $\eta_2 = \eta_1 \exp\left[-\frac{\Delta E}{k_B T}\right]$ and the

$$\text{self correlation function for anomalous diffusion } G_s^{diff}(r, t) = \exp\left[-\frac{r^2}{\left(4(Dt)^{\beta_{diff}} + \sigma^2 \right)} \right] / \tilde{V}.$$

σ is the width of the initial Gaussian distributions (actually two distributions were used which were kept fixed later on). The solid lines in Figure 14a and b present a fit of Eq.[26] to the data. Over the full time range the simple model describes the simulation data very accurately. The strong separation in time scales allows a separate stable fit of the overall sublinear diffusion characteristics and the hopping process.

The fit reveals an average jump distance for $1H_{trans}$ of 2.5\AA and for $1H_{cis}$ of $3 \pm 1\text{\AA}$. The evolving jump times are $\langle \tau_{hop}^{trans} \rangle = 2.6ns$ and $\langle \tau_{hop}^{cis} \rangle = 230ns$. The stretching exponents amount to $\beta_{hop}^{trans} = 0.5$ and $\beta_{hop}^{cis} = 0.6$ indicating broad distributions of hopping times. Finally, the fit reveals a weak asymmetry of the double well potential $\Delta_E \cong 1.2k_B T$ for $1H_{trans}$. The average jump time for $1H_{trans}$ is in the range of the experimental findings from the damping of the Brillouin modes and the secondary relaxation time from NSE. The jump distance $d_{trans} = 2.5\text{\AA}$ corresponds well to conformational jumps of the $1H_{trans}$ atom. The hopping time for a $1H_{cis}$ is much longer and remarkably close to the β relaxation time. We note that the cis unit carries the electric dipole moment. Aside of the hopping motion the broadening of the two peaks in the self correlation function reveals in anomalous diffusion process with $d = 2.2 \cdot 10^{-7} \text{\AA}^{2/\beta_{diff}} / ps$ and a stretching exponent $\beta_{diff} = 0.4$.

Fourier transformation of Eq.[26] yields the dynamic structure factor for self motion.

$$S_s(Q, t) = \exp\left[-\frac{Q^2 \sigma^2}{4}\right] \exp\left[-Q^2 (Dt)^{\beta_{diff}}\right] \times \left\{ \eta_1^2 + \eta_2^2 + 2\eta_1 \eta_2 \frac{\sin(Qd)}{Qd} + 2\eta_1 \eta_2 \left(1 - \frac{\sin(Qd)}{Qd}\right) \exp\left[-\left(\frac{t}{\tau_{hop}}\right)^{\beta_{hop}}\right] \right\} \quad (27)$$

Figure 15 displays the prediction of Eq.[27] for several Q values and compares them with the simulated structure factors. Obviously, the simple model reveals an overall very good description of the MD data and thus depicts all major dynamic features of the system. While in the real space the local jump dynamics is very well separated in time from the anomalous diffusion (α -relaxation) in Fourier space no evidence for a separate process other than an anomalous stretching appears. Finally, the dotted lines present predictions for the anomalous diffusion neglecting the hopping term. At all Q values strong deviations between the simulated structure factors and the predicted diffusion structure factors are evident. This holds even for low Q values where common wisdom would not suspect any influence from local motions. Figure 15 also includes a comparison with neutron spin echo data on PB which were obtained at 280K. There the anomalous diffusion is the overwhelming process and dominates strongly any local dynamics.

The insert in Figure 15 displays the Q dependent relaxation times obtained from a fit with a stretched exponential yielding a stretching exponent of $\beta_{diff} = 0.5$. As discussed in section 4.1 anomalous diffusion connects the shape of the relaxation function with the Q dispersion of the relaxation time as $\tau_{KWW} \approx Q^{-2/\beta_{diff}}$, a relation well fulfilled by the data. In order to compare with the simulations we first construct a master curve in scaling the time variable with Q^4 . Then we shift the α time scale with the known viscosity shift factor for PB. The resulting data points are also displayed in Figure 15 - the result is stunning. Without any further adjustment the shifted data agree with a predicted diffusion structure factor (α -relaxation) obtained from the modellisation of the simulation results. The experimental data however, do not agree with the fully simulated structure factor which includes the local dynamics. Thus, in a system

with important internal degrees of freedom displaying a dynamics well separated from the overall motional processes, the dynamics of such degrees of freedom have an important impact on the selfcorrelation function even in the low Q regime (see Figure 15 $Q = 0.5 \text{ \AA}^{-1}$ data).

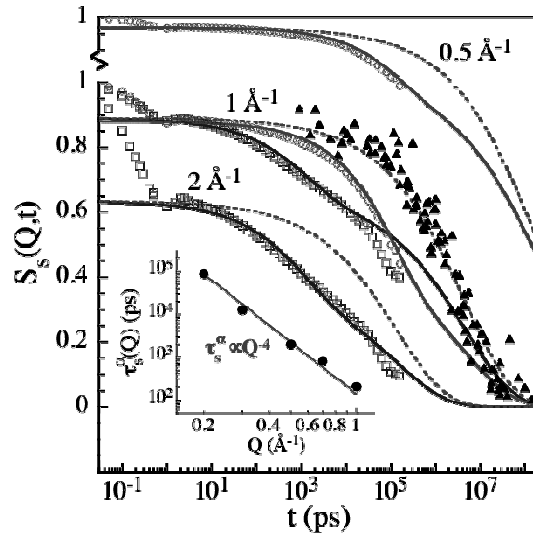


Fig. 15: $S_s(Q, t)$ obtained from the MD simulations at 200K for $1H_{trans}$ (squares, $Q = 1 \text{ \AA}^{-1}$ and 2 \AA^{-1}) and $1H_{cis}$ (circles, $Q = 0.5 \text{ \AA}^{-1}$ and 1 \AA^{-1}) atoms. The prediction of the model is shown by the solid lines and the dotted lines represent the contribution of the diffusion. The insert shows the Q -dependence of the characteristic times obtained from the NSE results at 280K; the solid lines is a description in terms of a Q^{-4} power law. The triangles represent the time temperature shifted NSE data corresponding to $Q = 1 \text{ \AA}^{-1}$ (see text).

6 Summary and conclusions

In this lecture we have demonstrated that atomistic MD simulations and neutron scattering reveal strongly related information which properly exploited leads to a deeper insight into atomic motions.

From the combination of atomistic MD simulations and experiments the α -relaxation in polyisoprene has been scrutinized and a simple picture of the motional process underlying the α -relaxation evolved.

- At low Q corresponding to large distances we deal with a homogenous sublinear diffusion process. This result is by now supported by a number of detailed investigations into the relationship between the shape of the relaxation function and the Q dispersion of the characteristic relaxation times also in other polymers.
- At higher Q the relationship between the shape and the dispersion relation demanded by Gaussianity breaks down and a weaker dispersion is found.
- This crossover in the Q dispersion of τ_{KWW} is related to a strong increase of the time dependent non-Gaussianity parameter $\alpha_2(t)$. It has been shown that typical relaxation

times measured with spectroscopic techniques are close to this crossover regime and therefore are effected by heterogeneity effects.

- The existence of the crossover clearly shows that the stretched exponential shape of the relaxation function cannot be explained entirely by heterogeneity but depending on length scale relates to intrinsic sublinear diffusion processes.
- In terms of a minimal model the changing Q dispersion may be explained in terms of a sublinear jump diffusion model, featuring a distribution of jump lengths. The distribution thereby seems to vary little with temperature. From this model a non-Gaussianity parameter $\alpha_2(t)$ may be calculated which agrees well with the simulation.
- This good agreement suggests that at least to a reasonable approximation the apparent non-Gaussianity observed for the α -process at short enough times is indeed a result of a local diffusion process with a distribution of finite jump length.

On glass forming polybutadiene close to the glass transition temperature T_g we have shown atomistic simulations and validated them in comparing with dynamic structure factor measurements. We have demonstrated that in case of well separated time scales the nature of the local dynamics is much more clearly revealed if the selfcorrelation function is evaluated in real space.

- There the radial selfcorrelation function reveals itself in terms of well separated diffusive and hopping contributions.
- In reciprocal space the two processes cannot be distinguished and give rise to an anomalous stretching of the relaxation function. Over the full Q regime the corresponding structure factor is strongly effected by the localized motions.

The approach demonstrates that the proper combination of real space analysis of simulations and neutron scattering experiments has the potential to yield deep insight into motional processes which are hidden if one only considers structure factors in Fourier space.

References

- [1] H. Sun, J. Comput. Chem. 15, 752 (1994); H. Sun, S.J. Mumby, J.R. Maple, A.T. Hagler, J. Am. Chem. Soc. 116, 2978 (1994); H. Sun, Macromolecules 28, 701 (1995); 26, 5924 (1994); H. Sun, S.J. Mumby, J.R. Maple, A.T. Hagler, J. Phys. Chem. 99, 5873 (1995)
- [2] D.N. Theodorou, U.W. Suter, Macromolecules 18, 1467 (1985); 19, 139 (1986); 19, 379 (1986)
- [3] F. Mezei, in *Neutron Spin Echo*, Lecture Notes in Physics, 28 (Springer Verlag, Heidelberg, 1980)
- [4] B. Farago, A. Arbe, J. Colmenero, R. Faust, U. Buchenau, D. Richter, Phys. Rev. E65, 051803 (2002)
- [5] A. Arbe, J. Colmenero, M. Monkenbusch, D. Richter, Phys. Rev. Lett. 81, 590 (1998)
- [6] A. Arbe, J. Colmenero, F. Alvarez, M. Monkenbusch, D. Richter, B. Farago, B. Frick, Phys. Rev. Lett. 89, 245701 (2002)
- [7] J. Colmenero, F. Alvarez, A. Arbe, Phys. Rev. E 65, 041804 (2002)
- [8] F. Alvarez, J. Colmenero, R. Zorn, L. Willner, D. Richter, Macromolecules 36, 238 (2003)
- [9] B. Frick, L.J. Fetters, Macromolecules 27, 974 (1994)
- [10] R. Graft R, A. Heuer A, Spiess HW (1998) Phys Rev Lett 80:5738
- [11] J. Colmenero, A. Arbe, F. Alvarez, A. Narros, M. Monkenbusch, and D. Richter, Europhysics Letters 71, 262 (2005).

For general reading:

- *Neutron spin echo in polymer systems*, D. Richter, M. Monkenbusch, A. Arbe, J. Colmenero, Advances in Polymer Science **174**, ISBN: 3-540-22862-4 (2005)
- *Introduction to the theory of thermal neutron scattering*, G.L. Squires, Cambridge University Press, Cambridge (1978)
- *Bridging the Gap between the atomistic and coarse-grained polymers; Status and perspectives*, J. Baschnagel, K. Binder, P. Doruker, A.A. Guser, O. Hahn, K. Kremer, W.L. Mattice, f. Müller-Plathe, M. Murat, W. Paul, S. Santos, U.W. Suter, V. Tres Advances in Polymer Science 41, 152 (2000)